Time-Domain Signature Chipless-RFID tags

Near-field chipless-RFID systems with high data capacity

[1]Cristian Herrojo, [2]Miquel Moras, [1]Ferran Paredes, [2]Alba Núñez, [3]Javier Mata-Contreras, [2]Eloi Ramon, [1]Ferran Martín

[1]CIMITEC, Departament d'Enginyeria Electrònica
Universitat Autònoma de Barcelona, 08193 Bellaterra (Barcelona), Spain
Corresponding author: Ferran.Martin@uab.es

[2] Institut de Microelectrònica de Barcelona, IMB-CNM (CSIC), 08193 Bellaterra, Spain

[3]Departamento de Ingeniería de Comunicaciones, Universidad de Málaga, 29016 Málaga, Spain

Chipless radiofrequency identification (chipless-RFID) technology has emerged in the last years as an alternative to RFID systems with tags equipped with silicon integrated circuits (ICs), or chips [1]-[12]. The main advantage of chipless-RFID systems over their chipped counterparts is the lower cost of the tags, motivated by the fact that the identification (ID) code is contained in a printed planar encoder (implementable with conductive inks), rather than being stored in a silicon chip. Low-cost tags (below the US $0.01 barrier) are necessary in many RFID applications involving tagged items or objects with moderate or low price, where chip-based tagging would represent a significant penalty in terms of overall costs. However, chipless-RFID systems present three main drawbacks, as compared to conventional (i.e., chip-based) RFID technology: (i) large tag size, (ii) limited data storage capacity, and (iii) shorter read-ranges. These negative aspects, and the fact that the materials (inks) and manufacturing processes (such as substrate functionalization or printing) needed for tag fabrication still do not represent a significant reduction in tag price (as compared to the cost of passive UHF-RFID tags, of the order of several cents), have limited the penetration of chipless-RFID technology in the market. In this article, an overview of the recent advances to increase the data density of printed encoders, with direct impact on tag size and data capacity, is carried out. Moreover, a recent chipless-RFID concept, based on near-field and sequential bit reading, providing very high data storage capacity (only limited by tag size), is discussed in detail. It is also pointed out that these novel chipless-RFID systems, with tag reading by proximity, are of special interest for security and

authentication applications, where reading at short distance from the tag provides system confidence against external interferences, spying, or eavesdropping.

CHIPLESS RFID VERSUS CHIPPED RFID AND OPTICAL BARCODES

Radiofrequency identification (RFID) is a wireless technology mainly used for identification and tracking of objects, goods, beings, animals and people. [13],[14]. Most commercially available RFID systems use identification (ID) tags equipped with silicon integrated circuits (IC), or chips, which contain the information relative to the tagged item. As compared to optical bar codes or QR codes, RFID tags are able to store significantly much more information, allowing the identification of individual items. RFID tags do not require direct line-of-sight with the reader, and reading distances of several meters are possible in far-field passive tags operating in the UHF band (UHF-RFID tags). Such distances can be extended up to dozens of meters in tags equipped with batteries (active tags), at the expense of higher tag cost and size. Despite the fact that passive UHF-RFID tags are relatively cheap (several US $ cents), its use is prohibitive in many applications involving low-cost tagged items. Tag cost is dictated by the presence and placement of the IC (by contrast tag size is determined by the antenna, needed for communication purposes with the reader), and it is difficult to envision a future scenario (at least at short term) where the prices of chipped tags drop to US $0.01 or below.

Chipless-RFID has emerged as an alternative technology to chip-based RFID to partially alleviate the high cost of silicon chips [1]-[12]. In chipless-RFID, the tags typically consist of a printed encoder and in some cases they are equipped with an antenna for communication with the reader. By replacing the ICs with such encoders, tag cost can be dramatically reduced, and reasonable predictions situate the cost of massively manufactured chipless-RFID tags below 1 cent [1]. In chipless-RFID, tag price is dictated by the (progressively decreasing) cost of conductive inks, and by the printing fabrication processes (rotogravure, rotary or planar screen-printing, inkjet). The final cost is mainly determined by the amount of ink required by the encoder (in turn related with the data storage capability, or number of bits), and by the tag antenna, if it is present.

Chipless-RFID tags are situated between chip-based tags and optical barcodes (or QR codes) in terms of performance (i.e., read range), and cost. Table 1 provides a comparison between these ID technologies that includes performance, cost, size, and other aspects, relevant in certain applications. According to the table, current chipless-RFID research drives the improvement in tag storage capacity, size, and read range (important limitations, as anticipated before, as compared to chipped RFID). Progress in any of these areas, combined with the low tag cost, low power needed by the reader, and robustness against harsh environments (due to the absence of electronic circuits [15]), may push chipless-RFID technology towards its progressive penetration in the market.

Table 1. Comparison between chipless-RFID tags, chipped RFID tags, and optical ID codes.

	Optical ID codes	**Chipless RFID**	**Chipped RFID**
Cost	Ultra low	Low	Medium
Size	Very small	Large	Medium
Read range	Very small	Small/moderate	High
Data storage	Medium	Medium	High
Simultaneous reading	No	No	Yes
Reprogrammable	No	Yes (with limits)	Yes
Single band operation	Yes	No	Yes
Power level (reader)	---	Low	Moderate
Harsh environment	No	Yes (with limits)	No
Easy to copy	Yes	No	No

An important aspect highlighted in Table 1, related to tag costs, concerns writing and erasing the tags, a feature which is not possible in optical barcodes or QR codes. By massively printing all-identical chipless tags, and programming them in a later stage, tag manufacturing costs can be reduced significantly, since a single mask is needed for that purpose. Tag programming (and erasing) is possible under certain circumstances, as will be discussed later, and it is a key factor for the potential success of chipless-RFID in future. However, it is not realistic to write/erase (reprogram) the ID code of the tags as many times as in chip-based tags. It is also not always possible to manufacture all-identical tags and then write the ID code in a later stage (e.g., if the code depends on the shape of the elements forming the encoder). For these main reasons, this aspect has been market as “Yes (with limits)” in Table 1.

Another important issue, very sensitive in applications devoted to security and authentication, is copying and plagiarism. Optical barcodes (or QR codes) can be simply photocopied, and the copy has exactly the same functionality as the original code. Therefore, low-cost copying is possible in optical ID systems; in contrast, copying of RFID tags (both chipless and chipped) is possible, but more sophisticated (and hence high cost) systems are needed for that purpose. Particularly, chipless-RFID tags based on printed conductive inks can be reverse-engineered (unless the encoders are buried), and consequently can be reproduced. However, to this end, high-cost printers, conductive inks, and custom printing processes are required. On the other hand, although photocopied chipless-RFID tags contain, indeed, the ID code, tag reading cannot be achieved by means of a specific (dedicated) chipless-RFID reader (able to read the ink-based printed tags). Thus, counterfeiting of items or goods is prevented, unless high-cost systems are used for copying.

Other differences between the considered wireless ID technologies are the possibility of simultaneous tag reading (only possible in chip-based RFID systems), the required power level of the reader (moderate in chipped RFID systems, as long as a minimum power level is needed to activate the chip), and the bandwidth of the interrogation signal

(narrow, i.e., single-band, in optical ID codes and chipped RFID systems, but wide in most chipless-RFID systems). Finally, for tag operation in harsh environments, it should be noted that silicon ICs exhibit limited robustness against extreme ambient factors (temperature, humidity, radiation). Therefore, chipless-RFID tags can be considered to be (in general) superior in this aspect, although the properties of conductive inks may be degraded if they are subjected to extreme conditions, as well. In certain environments subjected to pollution, the functionality of optical barcodes and QR codes may be limited, contrary to the superior robustness of RF systems against dirtiness.

CLASSIFICATION OF CHIPLESS-RFID SYSTEMS

A detailed classification of chipless-RFID systems (or tags) was previously given in [1]. It is now accepted that there are two main categories of printed chipless tags, i.e., time-domain based tags [16]-[25] and frequency-domain based tags [1],[2],[26]-[42], and a third group, where several domains are exploited simultaneously (hybrid tags) [43]-[56]. In addition to these types of tags, there is a recently reported approach for the implementation of chipless-RFID systems, where tags are read by proximity (through near-field) and sequentially [57]-[63]. This unconventional system exploits the time-domain, but the working principle is different than most chipless-RFID systems operating in the time domain. The main advantage of this approach is the achievable number of bits, which is only limited by tag size. The ID code is contained in the amplitude modulated signal generated by the tags, which can be considered to be time-domain signature barcodes, analogous to the frequency (or spectral) signature barcodes of frequency-domain based chipless-RFID tags [1]. Since these novel chipless-RFID systems are the main purpose of this article, we will study them separately in the next Section. We next review the cited approaches, in order to understand the potential of time-domain signature barcodes in terms of data capacity.

Time-domain based systems

The general working principle of time-domain based chipless-RFID systems is time domain reflectometry (TDR) –see Fig. 1. In these systems, the ID code is contained in the echoes generated by a delay line (with reflectors situated at certain positions corresponding to the specific ID code) to a pulsed interrogation signal. TDR based tags exhibit fast responses as compared to frequency-domain tags, but their bit encoding capability is limited, and either large delay lines or very narrow pulses are needed to avoid overlapping of the reflected pulses. Tags based on surface acoustic wave (SAW) technology [64]-[68] exhibit competitive performances, but at the expense of high cost, as long as a fully planar approach is not involved in this case (these tags need electro-acoustic transducers).

Frequency-domain (spectral signature) based systems

For the reasons explained before, most fully planar chipless-RFID tags are implemented on the basis of frequency-domain reading, rather than time-domain. Frequency-domain based tags, also designated as spectral signature barcodes, consist of a set of resonant

elements each one tuned to a different frequency. Typically, each resonant element provides a bit of information, and the corresponding logic state, '1' or '0', depends on whether the resonant element is functional or detuned (inoperative) at the fundamental frequency. Tag reading proceeds by sending a multi-frequency interrogation signal (covering the spectral bandwidth) to the tag, and the ID code is given by the presence or absence of abrupt spectral features either in the amplitude, phase or group delay responses. Figure 2 illustrates the working principle of frequency-domain chipless-RFID systems, where two types of tags can be considered: (i) retransmission-based [27],[28], [35] and (ii) backscattered-based [26],[33] tags. In the former, a transmission line is loaded with the encoding resonant elements, and it is equipped with two cross-polarized antennas for reception/transmission from/to the reader. In backscattered chipless tags, the resonant elements provide the spectral signature through the peaks in their radar cross section (RCS) response, and antennas are avoided, hence reducing the size of the tags.

Despite the fact that a considerable number of bits (35) has been reported in spectral signature chipless-RFID tags based on spiral resonators [27], see Fig. 3, the required spectral bandwidth for tag reading is very wide, and this represents a penalty in terms of reader costs in a real scenario, where the sweeping interrogation signal must be generated by means of a voltage-controlled oscillator (VCO). Strategies to increase the density of bits per frequency (DPF), exploiting more than one domain simultaneously, have been recently reported, giving rise to the so-called hybrid approach, to be discussed next.

Hybrid approach (enhancing the data density)

In hybrid tags, the main aim is to increase the number of bits by providing more than two logic states per resonant element, using simultaneously two independent parameters (or domains) for coding. By this method, the data density per frequency (DPF) and the data density per surface (DPS), two figures of merit in chipless tags, can be effectively improved. Various proposals for hybrid chipless-RFID tags can be found in the literature, including tags where frequency position is combined with phase deviation [43], polarization diversity [44], or notch bandwidth [55], and tags where the frequency is combined with the peak [48],[49] or notch [50],[51] magnitude, among others [45]-[47],[52]-[54],[56]. Hybrid tags use frequency for coding, and therefore they can be considered to be frequency domain tags, as well.

Let us illustrate the potential of hybrid tags with two examples. In [43], Vena *et al*. achieved a coding capacity equivalent to 22.9 bits with only five resonant elements, by combining frequency position with phase deviation. The authors used C-shaped resonators, with resonance frequencies in the range 2.5 GHz – 7.5 GHz, printed on *FR4* substrate (Fig. 4). The principle is based on the RCS responses of these resonant elements, which exhibit a peak and a dip. The peak frequency depends on the length of the resonant element, whereas the dip position is given by the ratio g/L, with g and L defined in Fig. 4. Figure 5 depicts the four responses inferred from a single resonant

element, by slightly modifying its dimensions. For each resonance peak, there are two dips that provide different phase response. This example shows that a single resonant element can implement at least two bits. Therefore, by allowing further variations in the dimensions, it is possible to enhance the coding capacity per resonant element (4.6 bits per resonant element in [43]).

Another possibility mentioned before and reported here as a second illustrative example, exploits the magnitude level of the RCS of C-shaped resonant elements [49]. The tags are very similar to those of the previous example, but in this case the modulation in the resonator dimensions is focused on varying the peak level of the RCS. Figure 6 depicts three different tags, together with the measured responses (RCS magnitude level) of the three first peaks, showing the potential in generating multiple states per resonant element. Within this approach, 3 bits per resonant element are achievable, according to the authors [49].

Although hybrid coding techniques provide enhanced data density per frequency, an intrinsic limitation is related to the fact that resonator bandwidth requirements increase as the number of bits per resonant element increases. In other words, to achieve dozens of bits (but still far from the data capacity of chipped tags), significant fractional bandwidths are needed. In [43] the fractional bandwidth occupied by the tags is as high as 100%, and only 22.9 bits are achieved, i.e., very far from the 96 bits of UHF-RFID tags, according to the electronic product code (EPC) tag data standard. In [45], 64 bits are achieved, but with a spectral bandwidth of 6.4 GHz. Let us review in the next section a recently proposed approach, useful in increasing the number of bits, where the interrogation signal is simply a harmonic (single-tone) signal. Tag reading by proximity (near-field) is a due, but this is not necessarily an issue in applications related to security and authentication, as will be discussed.

VERY HIGH DATA-STORAGE CAPACITY TAGS: TIME-DOMAIN SIGNATURE NEAR-FIELD CHIPLESS-RFID SYSTEMS

The first proposals for chipless-RFID systems based on frequency-domain were based on the presence or absence of resonant elements tuned at the predefined frequencies within the spectral bandwidth, or, equivalently, on the basis of the functionality or not (detuning) of such resonant elements [27],[28]. Within this approach, the tag ID code is "frequency distributed", and this represents a penalty in terms of reader costs, as long as a wideband interrogation signal is required for tag reading. Alternatively, this resonator presence/absence based scheme (or resonator functionality/detuning) can be implemented in the time domain, by considering identical resonators (functional or detuned, depending on the logic state) that are read sequentially (i.e., at different time) [57]-[63]. The resonant elements forming the code must be simply grouped forming a chain, and its functionality (and hence the ID code) can be detected through near-field, by displacing the resonator chain (the tag) over the active part of the reader, and in close proximity to it. According to this strategy, the ID code is "time distributed"; to be more precise, we should say that both the frequency-domain encoders and these novel time-

domain encoders contain the ID code distributed in space. However, tag reading proceeds by frequency sweeping in the former case, and by time-division multiplexing in the second case. Conceptually, both systems are similar, but in the novel proposed chipless-RFID system, the required spectral bandwidth is small, since a (single-tone) harmonic interrogation signal, tuned to the frequency of the resonators (or close to it), is required for tag reading, as will be shown. Usually, frequency-domain chipless-RFID tags are designated as spectral (or frequency) signature barcodes. Similarly, these novel time-domain chipless tags based on chains of identical (functional or detuned) resonators can be designated as time-domain signature barcodes.

In order to sequentially detect the functional and detuned resonators of the chain through near-field, as required in a reading operation, an element sensitive to electromagnetic coupling with the resonant elements of the tag, e.g., a transmission line, is needed. By feeding such line (active part of the reader) with a harmonic signal tuned to the frequency of the tag resonators (or close to it), the presence of functional resonators very close to the line will generate line-to-resonator coupling, which in turn will modify (decrease) the transmission coefficient. Consequently, by displacing the tag chain over the line (next to it), the amplitude of the feeding signal will be modulated at the output port of the line according to the presence or absence of functional resonators, and hence the ID code can be inferred from the amplitude-modulated (AM) signal. The interrogation signal being a single-tone (carrier) signal, causes the system to operate in a similar fashion as an AM modulator, and the ID code is given by the envelope function, which can be obtained by means of an envelope detector. The working principle of this time-domain chipless-RFID system is illustrated in Fig. 7.

Let us now discuss the tag reader. By simply using a transmission line (microstrip, CPW, etc.) as the sensitive element for tag reading through electromagnetic coupling (near-field), a fundamental limitation arises. In order to accommodate the largest possible number of bits per area unit, the distance between adjacent resonators in the tag must be reduced as much as possible (within the limits of the fabrication technology). Under these circumstances, both inter-resonator coupling in the tag chain (similar to the coupling that takes place in magneto-inductive wave transducers [69]) and multiple couplings between the line and several tag resonators (those closest to the line) cannot be avoided. These couplings can obscure the detection of the functional and detuned resonators, hence limiting the readability of the system, as discussed in [57]. Therefore, a solution to prevent such undesired effects (couplings) must be introduced, in order to achieve a high information density per surface (a figure of merit) by minimizing inter-resonator distance.

The strategy to solve the previous problem is to introduce a resonant element (identical to those of the tag chain) in the transmission line of the reader, and coupled to it (this solution was first introduced in [70],[71], for implementing angular velocity sensors based on chains of resonant elements). This generates a transmission zero (or notch) in the transmission coefficient of the line. The frequency position of this notch can be modulated by coupling the resonator of the line to an identical resonator. If the tag

resonators chain is displaced in close proximity to the resonator of the line, and the feeding (carrier) signal is tuned to the frequency of the notch that results from the coupling between both resonators (the one of the line and the one of the chain, provided it is functional), the previous undesired multiple couplings are avoided. The reason is that such couplings occur at the frequency of the isolated resonators, different from the one of the coupled resonators, which is smaller. The coupling between resonant elements may also limit the robustness of frequency-domain based systems. A solution for backscatter systems with tags based on U-shaped strips was reported in [72], where the authors propose the spatial rearrangement of individual tag scatterers to avoid such coupling effects.

The first tag prototypes based on this time-domain approach were implemented by means of S-shaped split ring resonators (S-SRRs), a structure first reported in [73]-[75], and later used in the design of angular velocity sensors [76]. The reader necessary to obtain the ID codes was based on an S-SRR loaded line, using a CPW (Fig. 8) [57]. This resonant element exhibits high magnetic coupling to the CPW at the fundamental resonance since the currents are antiparallel in each loop (one clockwise and the other one counterclockwise) at that frequency [76]. The S-SRR can be easily excited by the counter magnetic fields present at both slots of the CPW transmission line. By considering a gap distance between the S-SRR of the line and the one of tag of 0.25 mm, the fundamental resonance frequency of the coupled and perfectly aligned S-SRRs is found to be $f_0 = 4$ GHz (the considered substrates for the CPW and tag are indicated in the caption of Fig. 8). By tuning the feeding interrogation signal to that frequency, $f_c = f_0$, the excursion experienced by the transmission coefficient by tag motion is depicted in Fig. 9. The transmission coefficient is a minimum (with measured –6 dB transmission) in the reference position (perfectly aligned S-SRRs) and is a maximum (close to 0 dB transmission) when the relative displacement between the S-SRRs of the line and tag is half a chain period. By varying the gap distance, inevitable in a real scenario, the response of Fig. 9 changes, but there is some tolerance in the excursion experienced by the measured transmission coefficient (6 dB in Fig. 9). This excursion has direct impact on the modulation index of the output signal, and so is a key parameter in these time-domain chipless-RFID systems.

In [58], the S-SRR based tag and reader system was validated by considering circularly-shaped 40-bit tags, whereas in [60] a double linear chain of S-SRRs was considered in order to reduce the length of the tags. In the latter case, a pair of S-SRRs loading the CPW is needed, but the operation principle is exactly the same. Fig. 10 depicts the experimental set-up used to read the ID codes by means of an oscilloscope. Note that the envelope detector diode is preceded by an isolator (implemented by means of a circulator) in order to avoid unwanted reflections due to the high nonlinearity of the diode. The responses of different tags, with the indicated codes, are depicted in Fig. 11. The different codes have been inferred by cutting certain resonators in a unique fabricated tag (shown in Fig. 10), hence detuning them and making them inoperative, and so, tag programming is demonstrated. The number of bits achievable with this

approach is only limited by tag size, provided the mechanical system is able to displace the whole tag over the S-SRR-loaded line of the reader.

To provide further robustness to this type of chipless-RFID systems, it is convenient to expand the excursion experienced by the transmission coefficient at the frequency of the interrogation signal as much as possible. For that purpose, a reader based on a SRR-loaded microstrip line in a bandpass configuration was proposed in [61] (Fig. 12). The singularity of this topology is that it exhibits a pass band followed by a transmission zero. By loading this structure with a tag based on identical SRRs but oppositely oriented, i.e., rotated 180°, the transmission coefficient shifts to lower frequencies. Through a proper design, it is possible to match the transmission zero of the tag-loaded structure (with perfect alignment between the SRR of the reader and one SRR of the tag, REF position) to the frequency of maximum transmission of the unloaded reader, f_0, as Fig. 13 illustrates. This frequency, f_0, is roughly the same as the one corresponding to maximum transmission in the reader loaded with a completely misaligned tag (i.e., with the tag displaced ±3.16 mm with regard to the REF position). By these method, a significant excursion of the transmission coefficient at f_c is achieved (roughly 45 dB), provided f_c is tuned to f_0. This excursion is much larger than the one of the previously discussed system, based on an S-SRR-loaded CPW reader. In [61], circularly-shaped 40-bit tags were implemented in low-loss commercial microwave substrates, and linear 10-bit tags were fabricated by inkjet printing in plastic substrate, i.e., polyethilene naphthalate (PEN) film (*Dupont Teijin Q65HA*). The functionality of the system to read both types of tags was demonstrated in [61].

The latest advances concerning these time-domain signature tags and chipless-RFID systems have been recently achieved by implementing programmable/erasable 40-bit tags with header bits on *PowerCoat*^{TM} *HD ultra smooth* paper substrate (with thickness $h = 215\ \mu$m, measured dielectric constant and loss factor of $\varepsilon_r = 3.11$ and $\tan\delta = 0.039$, respectively) [62]. The resonant elements of the tags were printed by inkjet, and the topology of such resonators is identical to the one of the SRRs of Fig. 12. The same reader can be used to infer the ID codes, regardless of the specific substrate type and metallic layer (copper or conductive ink). The fabricated reader and tag (with all SRRs functional, i.e., all providing the logic state '1') are depicted in Fig. 14. The responses of this tag, with SRRs faced up or down (distinguished thanks to the header bits), after programming several codes, are depicted in Fig. 1 (the header bits are responsible for determining the sequence of reading, from left to right or vice versa). Tag programming was achieved by cutting certain resonators, providing the logic state '0'. Tag erasing can be achieved by short-circuiting previously cut resonators by adding conductive ink. This was done in [62], in order to recover the original ID code, and the resulting response (Fig. 16) exhibits the expected 40 dips of the ID code with all bits set to '1' (plus the additional dips corresponding to the header bits). Implementing these tags on a paper substrate, indicates that secure paper is a canonical application of this time-domain chipless-RFID system, based on near-field and sequential bit reading. By printing a coded chain of resonant elements in the border of a certain document (e.g., an official or

corporate document, certificate, ballot or exam), security against counterfeiting is provided at low cost. As an example, in the tag of Fig. 14, a single layer of conductive ink, with thickness of roughly 2.5 μm, was printed. Note that the elongated shape factor of the tags is not expected to represent a limitation in such applications. The results of Fig. 15 and 16 demonstrate that tag programming and erasing is possible, further reducing fabrication costs, as long as all identical tags can be massively fabricated (requiring only a single mask), and then programmed, e.g., by means of low cost printers, in a later stage (custom level).

One area of concern is system reliability, with an issue being mechanical friction, or wearing. In many secure paper applications (e.g., corporate documents or certificates), this is not a true limitation, provided such documents are not expected to suffer from wearing effects. However, in banknotes, for instance, typically subjected to wearing or aging, the reliability of the system cannot be guaranteed. In terms of the bit error rate, a typical performance indicator in digital data transmission, related to noise or interference effects, the system outlined in [57]-[63] is quite robust against reading errors, provided the mechanical system used to guide the tag over the reader guarantees a maximum tag distance and proper alignment.

In [62], the ID codes were observed in an oscilloscope and the feeding signal was generated by means of a commercial function generator. The relative motion between the tag and the reader was achieved by means of a mechanical guiding system (based on a step motor) providing either circular (for the circularly shaped tags) or linear (for the linear tags) displacement [Fig. 10(a)]. In the last proof-of-concept demonstrator, a printer was adapted and equipped with an *adhoc* guiding channel in order to absorb the tag (document with the printed encoder). This system guarantees good alignment and roughly constant air gap distance between the tag chain and the resonator of the reader, also conveniently placed and adapted to the modified printer. The envelope detector, implemented by means of a diode, an active probe (with resistance and capacitance R = 1 MΩ and C = 1 pF, respectively) and an isolator, to prevent reflections from the diode, in the experimental setup shown in Fig. 10, is replaced with an integrated circuit (*Analog Devices ADL5511*) able to provide the envelope function (hence reducing costs). Such an envelope signal is then sent to a data acquisition card (*National Instruments myRIO*), where the sampled data can be viewed (the read speed is limited by the sampling rate, but typical sampling rates are sufficiently high to ensure tag readability even with mechanical systems providing a fast tag motion). The photograph of this experimental setup is shown in Fig. 17. From the sampled data the ID code can be easily inferred by means of a simple post-processing scheme, able to detect the notches. This setup has been used in [63] to read 80-bit (plus the header bits) chipless-RFID tags inkjet printed on ordinary (and low cost) DIN A4 paper. The photograph of the printed tag, with all bits set to ‘1’ is shown in Fig. 18. Reading such codes with both tag orientations (face up and down) has produced the responses depicted in Fig. 19(a). Tag programming was performed by cutting (detuning) some resonant elements, effectively writing the ‘0’ logic state in the corresponding resonator. The resulting code

and responses are shown in Fig. 19(b), where the functionality and validity of the system can be appreciated. These latter results, which represent a significant advance as compared to the first time-domain near-field chipless-RFID system prototype reported in [57], are important since the functionality of the system is demonstrated by considering chipless tags printed on ordinary and low-cost paper. The reported time-domain signature barcodes may find application in many diverse scenarios involving the use of ordinary paper equipped with printed ID codes for identification and authentication purposes.

Similar to frequency-domain chipless-RFID systems, which can be applied to sensors [77]-[84], the proposed time-domain near-field chipless-RFID system can be also used for sensing purposes (e.g., proximity sensors with ID code [85], or motion control devices [70],[71]), but such applications are out of the scope of this article, entirely focused on identification.

COMPARATIVE ANALYSIS AND CONCLUSIONS

In this article, we have discussed several strategies for the implementation of chipless-RFID systems, including time-domain reflectometry (TDR), frequency-domain spectral signature barcodes, and several approaches where different domains are exploited simultaneously in order to increase the information density (or number of bits) per spectral bandwidth. Despite the fact that several frequency-domain and hybrid systems where various bits of information per resonant element of the tag have been reported, an intrinsic limitation in the achievable number of bits is related to the bandwidth occupied by each resonator. Such bandwidth, which increases as the data capacity of the resonant elements increases, cannot exceed certain limits in order to avoid an excessive cost of the reader (which must generate a multi-frequency sweeping interrogation signal for tag reading). To solve the previous limitation, a time-domain chipless-RFID approach, where tags are read through near-field coupling (with sequential bit reading) by means of a harmonic interrogation signal, has been recently reported, and such an approach has been reviewed in this article. Validation examples have been discussed and reported, including tag implementation in commercially available substrates and also on paper substrates, where the tags have been printed by inkjet.

A comparative analysis of the main characteristics of the different chipless-RFID systems is given in Table 2, where the most representative figure of merit of the whole considered approaches is the number of bits per surface area (DPS). The total number of bits is also a relevant parameter, limited by the occupied spectral bandwidth of the tags in frequency-domain or hybrid systems, and by the length of the delay lines and bandwidth of the pulsed interrogation signal in TDR-based tags. In a system based on time-domain signature tags with near-field and sequential bit reading, the main objective of this article, a very high DPS can be achieved.

Table 2. Comparative analysis of various chipless-RFID tags.

Ref.	Bandwidth (GHz)	Bits	Area (cm^2)	DPF (bit/GHz)	DPS (bit/ cm^2)/DPL (bits/cm) **
Time-domain (Pulsed interrogation signal)					
[16]	---	4	59.4	---	0.07/0.02
[20]	0.05	2	---	40	---/0.10
[22]	---	4	---	---	---/0.06
[23]	---	8	---	---	---/0.20
[24]	0.8	5	26	6.25	0.19/0.19
[25]	---	2	70.0	---	0.03/---
[53]	---	2	8.75	---	0.23/---
Time-domain (Harmonic interrogation signal)					
[58]	*	40	5.40	*	7.4/3
[63]	*	80	9.44	*	8.47/3
Frequency-domain					
[26]	1	5	6.48	11.1	0.77
[27]	7.5	35	57.2	8.97	0.61
[29]	0.2	5	50.1	25.0	0.10
[32]	2	20	17.5	10.0	1.14
[33]	3.5	9	3.00	2.57	3.00
[34]	7.5	19	9.00	2.53	2.11
[36]	7	28.5	8.00	4.07	3.56
[37]	7.5	24	5.76	3.20	4.17
[41]	1.2	20	17.5	16.7	1.14
Hybrid					
[43]	5	22.9	8.00	4.58	2.86
[45]	6.4	64	10.9	10.0	5.88
[51]	1	16	6.75	16.0	2.37
[49]	3	9	7.20	3.00	1.25

* The spectral bandwidth of this approach is virtually null due to the fact that the interrogation signal is harmonic.

** In time-domain tags, the density of bits per unit length (DPL) is sometimes given, specially in tags based on delay lines.

The unprecedented number of bits in chipless-RFID technology (a 80-bit system with 4 header bits [63]) can be achieved since that the data storage capacity in such chipless-

RFID tags is only limited by tag size. In summary, the time-domain chipless-RFID approach discussed can provide very competitive performance in terms of data capacity and size at the expense of tag reading by proximity (near-field). This proximity between the tag and the reader may be of interest in some applications. This novel and unconventional system may be of special interest in applications involving secure paper, where tag reading by proximity may represent an added value in terms of confidence against gathering or spying.

ACKNOWLEDGMENTS

This work was supported by MINECO-Spain (projects TEC2016-75650-R, TEC2014-59679-C2-1-R and RTC-2014-2550-7), *Generalitat de Catalunya* (project 2017SGR-1159), *Institució Catalana de Recerca i Estudis Avançats* (who awarded F. Martín), and by FEDER funds. C. Herrojo acknowledges MINECO for supporting his research activity through the FPI grant BES-2014-068164.

References

1. S. Preradovic and N. C. Karmakar, "Chipless RFID: bar code of the future," *IEEE Microwave Magazine*, vol. 11, pp. 87-97, 2010.
2. S. Preradovic and N. C. Karmakar, *Multiresonator-Based Chipless RFID: Barcode of the Future*, Springer, 2011.
3. N.C. Karmakar, R. Koswatta, P. Kalansuriya, R. E-Azim, *Chipless RFID Reader Architecture*, Artech House, 2013.
4. E. Perret, *Radio Frequency Identification and Sensors: From RFID to Chipless RFID*, John Wiley, New York, 2014.
5. R. Rezaiesarlak, M. Manteghi, *Chipless RFID: Design Procedure and Detection Techniques*, Springer, 2015.
6. N. C. Karmakar, M. Zomorrodi, C. Divarathne, *Advanced Chipless RFID*, John Wiley, Hoboken, NJ, 2016.
7. S. Tedjini, N. Karmakar, E. Perret, A. Vena, R. Koswatta, and R. E-Azim, "Hold the chips: chipless technology, an alternative technique for RFID," *IEEE Microw. Mag*., vol. 14, no. 5, pp. 56–65, Jul. 2013.
8. N. C. Karmakar, "Tag, You're it radar cross section of chipless RFID tags," *IEEE Microw. Mag*., vol. 17, no. 7, pp. 64–74, Jul. 2016.
9. S. Dey, J. K. Saha, and N. C. Karmakar, "Smart sensing: chipless RFID solutions for the internet of everything," *IEEE Microw. Mag*., vol. 16, no. 10, pp. 26–39, Nov. 2015.
10. B. Shao, Q. Chen, Y. Amin, R. Liu, and L.-R. Zheng, "Chipless RFID tags fabricated by fully printing of metallic inks," *Ann. Telecommun. - Ann. Télécommunications*, vol. 68, no. 7–8, pp. 401–413, Aug. 2013.
11. A. Vena, E. Perret, and S. Tedjini, "Design rules for chipless RFID tags based on multiple scatterers," *Ann. Telecommun. - Ann. Télécommunications*, vol. 68, no. 7–8, pp. 361–374, Aug. 2013.
12. M. Forouzandeh and N. C. Karmakar, "Chipless RFID tags and sensors: a review on time-domain techniques," *Wirel. Power Transf*., vol. 2, no. 2, pp. 62–77, Oct. 2015.
13. K. Finkenzeller, *RFID Handbook: Radio-Frequency Identification Fundamentals and Applications*, 2nd Ed. New York, NY, USA: Wiley, 2004.
14. V. D. Hunt, A. Puglia, and M. Puglia, *RFID: A Guide to Radio Frequency Identification*, New York, NY, USA, Wiley, 2007.
15. S. Moscato *et al*., "Chipless RFID for space applications", 2014 *IEEE International Conference on Wireless for Space and Extreme Environments* (WiSEE), Noordwijk, Netherlands, Oct. 2014.
16. A. Chamarti and K. Varahramyan, "Transmission delay line based ID generation circuit for RFID applications," *IEEE Microw. Wireless Compon. Lett.*, vol. 16, pp. 588-590, 2006.
17. M. Schüßler, C. Damm, and R. Jakoby, "Periodically LC loaded lines for RFID backscatter applications," in Proc. of *Metamaterials 2007*, Rome, Italy, October 2007, pp. 103-106.

18. M. Schüßler, C. Damm, M. Maasch, and R. Jakoby, “Performance evaluation of left-handed delay lines for RFID backscatter applications,” in Proc. of the *IEEE MTT-S International Microwave Symposium 2008*, pp. 177-180.
19. B. Shao, Q. Chen, Y. Amin, D. S. Mendoza, R. Liu, and L.-R. Zheng, “An ultra-low-cost RFID tag with 1.67 Gbps data rate by ink-jet printing on paper substrate,” in *IEEE Asian Solid State-Circuits Conf*., 2010, pp. 1–4.
20. F.J. Herraiz-Martínez, F. Paredes, G. Zamora, F. Martín, and J. Bonache, “Printed magnetoinductive-wave (MIW) delay lines for chipless RFID applications”, *IEEE Trans. Ant. Propag.*, vol. 60, pp. 5075-5082, Nov. 2012.
21. S. Tedjini, E. Perret, A. Vena, D. Kaddout, “Mastering the electromagnetic signature of chipless RFID tags”, in *Chipless and Conventional Radiofrequency Identification*, ed. IGI Global, 2012.
22. L. Zhang, S. Rodriguez, H. Tenhunen, and L.-R. Zheng, “An innovative fully printable RFID technology based on high speed time-domain reflections,” in *Conference on High Density Microsystem Design and Packaging and Component Failure Analysis, 2006. HDP’06*., Shanghai, China, Jun. 2006, pp. 166–170.
23. L. Zheng, S. Rodriguez, L. Zhang, B. Shao, and L.-R. Zheng, “Design and implementation of a fully reconfigurable chipless RFID tag using Inkjet printing technology,” in *2008 IEEE International Symposium on Circuits and Systems*, Seattle, USA, May 2008, pp. 1524–1527.
24. C. Mandel, M. Schussler, M. Maasch, and R. Jakoby, “A novel passive phase modulator based on LH delay lines for chipless microwave RFID applications,” in *2009 IEEE MTT-S International Microwave Workshop on Wireless Sensing, Local Positioning, and RFID*, Cavtat, Croatia, Sep. 2009, pp. 1–4.
25. R. Nair, E. Perret, and S. Tedjini, “Temporal multi-frequency encoding technique for chipless RFID applications,” in *IEEE MTT-S International Microwave Symposium Digest*, Montreal, Canada, Jun. 2012, pp. 1–3.
26. I. Jalaly and I. D. Robertson, “RF barcodes using multiple frequency bands,” in *IEEE MTT-S International Microwave Symposium Digest*, Long Beach, USA, Jun. 2005, pp. 139–142.
27. S. Preradovic, I. Balbin, N. C. Karmakar, and G. F. Swiegers, "Multiresonator-based chipless RFID system for low-cost item tracking," *IEEE Trans. Microw. Theory Techn.*, vol. 57, pp. 1411-1419, 2009.
28. S. Preradovic and N. C. Karmakar, "Design of chipless RFID tag for operation on flexible laminates," *IEEE Anten. Wireless Propag. Lett.*, vol. 9, pp. 207-210, 2010.
29. J. McVay, A. Hoorfar, and N. Engheta, “Space-filling curve RFID tags,” in Proc. of *2006 IEEE Radio Wireless Symp.*, pp. 199–202.
30. I. Jalaly and D. Robertson, “Capacitively-tuned split microstrip resonators for RFID barcodes,” in Proc. of *European Microwave Conference*, October 2005, vol. 2, pp. 4–7.
31. H.-S. Jang, W.-G. Lim, K.-S. Oh, S.-M. Moon, and J.-W. Yu, “Design of low-cost chipless system using printable chipless tag with electromagnetic code”, *IEEE Microw. Wireless Compon. Lett.*, vol. 20, pp. 640-642, 2010.
32. A. Vena, E. Perret, and S. Tedjini, “A fully printable chipless RFID tag with detuning correction technique”, *IEEE Microw. Wireless Compon. Lett.*, vol. 22(4), pp. 209-211, 2012.
33. A. Vena, E. Perret, and S. Tedjini, “Design of compact and auto-compensated single-layer chipless RFID tag”, *IEEE Trans. Microw. Theory Techn*., vol. 60(9), pp. 2913-2924, Sep. 2012.
34. A. Vena, E. Perret, and S. Tedjini, “High-capacity chipless RFID tag insensitive to the polarization”, *IEEE Trans. Ant. Propag.*, vol. 60(10), pp. 4509-4515, Oct. 2012.
35. D. Girbau, J. Lorenzo, A. Lazaro, C. Ferrater, and R. Villarino, “Frequency-coded chipless RFID tag based on dual-band resonators,” *IEEE Ant. Wireless Propag. Lett*., vol. 11, pp. 126–128, 2012.
36. M. M. Khan, F. A. Tahir, M. F. Farooqui, A. Shamim, H. M. Cheema, "3.56-bits/cm^2 compact inkjet printed and application specific chipless RFID tag," *IEEE Ant. Wireless Propag. Lett*., vol. 15, pp. 1109-1112, 2016.
37. R. Rezaiesarlak and M. Manteghi, "Complex-natural-resonance-based design of chipless RFID tag for high-density data," *IEEE Trans. Ant. Propag.*, vol. 62, pp. 898-904, Feb. 2014.
38. M. S. Bhuiyan and N. Karmakar, “A spectrally efficient chipless RFID tag based on split-wheel resonator,” in *Int. Antenna Technol. Workshop on Small Antennas, Novel EM Struct., Mater., Appl*., 2014, pp. 1–4.
39. C. M. Nijas *et al*., “Low-cost multiple-bit encoded chipless RFID tag using stepped impedance resonator,” *IEEE Trans. Ant. Propag*., vol. 62, no. 9, pp. 4762–4770, Sep. 2014.
40. J. Machac and M. Polivka, “Influence of mutual coupling on performance of small scatterers for chipless RFID tags,” in *24th Int. Radioelektron. Conf*., 2014, pp. 1–4.

41. M. Svanda, J. Machac, M. Polivka, J. Havlicek., "A comparison of two ways to reducing the mutual coupling of chipless RFID tag scatterers," in Proc. of *21st International Conference on Microwave, Radar and Wireless Communications (MIKON)*, May 2016, pp. 1-4.
42. C. Herrojo, J. Naqui, F. Paredes and F. Martín, "Spectral signature barcodes based on S-shaped Split ring resonators (S-SRR)", *EPJ Applied Metamaterials*, vol. 3, pp. 1-6, Jun. 2016.
43. A. Vena, E. Perret, S. Tedjini, "Chipless RFID tag using hybrid coding technique," *IEEE Trans. Microw. Theory Techn.*, vol. 59, pp. 3356-3364, Dec. 2011.
44. A. Vena, E. Perret, S. Tedjini, "A compact chipless RFID tag using polarization diversity for encoding and sensing", *2012 IEEE Int. Conf. RFID*, pp. 191-197, 2012.
45. M. A. Islam and N. C. Karmakar, "A novel compact printable dual-polarized chipless RFID system," *IEEE Trans. Microw. Theory Techn.*, vol. 60, pp. 2142-2151, Jul. 2012.
46. I. Balbin, N.C. Karmakar, "Phase-encoded chipless RFID transponder for large scale low cost applications", *IEEE Microw. Wireless. Compon. Lett.*, vol. 19, pp. 509-511, 2009.
47. S. Genovesi, F. Costa, A. Monorchio, G. Manara, "Chipless RFID tag exploiting multifrequency delta-phase quantization encoding", *IEEE Ant. Wireless Propag. Lett.*, vol. 15, pp. 738-741, 2015.
48. O. Rance, R. Siragusa, P. Lemaitre-Auger, and E. Perret, "RCS magnitude coding for chipless RFID based on depolarizing tag," in *IEEE MTT-S Int. Microw. Symp. Dig*., 2015, pp. 1–4.
49. O. Rance, R. Siragusa, P. Lemaître-Auger, E. Perret, "Toward RCS magnitude level coding for chipless RFID," *IEEE Trans. Microw. Theory Techn.*, vol. 64, pp. 2315-2325, Jul. 2016.
50. C. Herrojo, J. Naqui, F. Paredes, F. Martín, "Spectral signature barcodes implemented by multi-state multi-resonator circuits for chipless RFID tags", *IEEE MTT-S International Microwave Symposium* (IMS'16), San Francisco, May 2016.
51. C. Herrojo, F. Paredes, J. Mata-Contreras, S. Zuffanelli and F. Martín, "Multi-state multi-resonator spectral signature barcodes implemented by means of S-shaped Split Ring Resonators (S-SRR)", *IEEE Trans. Microw. Theory Techn.*, vol. 65, no. 7, pp. 2341-2352, Jul. 2017.
52. S. Gupta, B. Nikfal, and C. Caloz, "Chipless RFID system based on group delay engineered dispersive delay structures," *IEEE Ant. Wireless Propag. Lett*., vol. 10, pp. 1366–1368, 2011.
53. R. Nair, E. Perret, and S. Tedjini, "Chipless RFID based on group delay encoding," in *IEEE Int. RFID-Technol. Appl. Conf*., 2011, pp. 214–218.
54. C. Feng, W. Zhang, L. Li, L. Han, X. Chen, and R. Ma, "Angle-based chipless RFID tag With high capacity and insensitivity to polarization," *IEEE Trans. Ant. Propag*., vol. 63, no. 4, pp. 1789–1797, Apr. 2015.
55. A. El-Awamry, M. Khaliel, A. Fawky, M. El-Hadidy, and T. Kaiser, "Novel notch modulation algorithm for enhancing the chipless RFID tags coding capacity," in *IEEE Int. RFID Conf*., 2015, pp. 25–31.
56. A. Vena, A. A. Babar, L. Sydanheimo, M. M. Tentzeris, and L. Ukkonen, "A novel near-transparent ASK-reconfigurable inkjet-printed chipless RFID tag," *IEEE Ant. Wireless Propag. Lett*., vol. 12, pp. 753–756, 2013.
57. C. Herrojo, J. Mata-Contreras, F. Paredes, Ferran Martín, "Near-field chipless RFID encoders with sequential bit reading and high data capacity", *IEEE MTT-S Int. Microw. Symp.* (IMS'17), Honolulu, Hawaii, June 2017.
58. C. Herrojo, J. Mata-Contreras, F. Paredes, F. Martín, "Microwave encoders for chipless RFID and angular velocity sensors based on S-shaped split ring resonators (S-SRRs)", *IEEE Sensors J*., vol. 17, pp. 4805-4813, Aug. 2017.
59. C. Herrojo, J. Mata-Contreras, F. Paredes, A. Núñez, E. Ramón, F. Martín, "Near-field chipless-RFID tags with sequential bit reading implemented in plastic substrates", *Int. J. Magnetism. Magnetic Mat*., published online, https://doi.org/10.1016/j.jmmm.2017.10.005.
60. C. Herrojo, J. Mata-Contreras, F. Paredes, F. Martín, "High data density and capacity in chipless radiofrequency identification (chipless-RFID) tags based on double-chains of S-shaped split ring resonators (S-SRRs)", *EPJ Appl. Metamat.*, vol. 4, article 8, 6 pages, Oct. 2017.
61. C. Herrojo, J. Mata-Contreras, F. Paredes, Ferran Martín, "Near-field chipless RFID system with high data capacity for security and authentication applications", *IEEE Trans. Microw. Theory Techn*., vol. 65 (12), pp. 5298-5308, Dec. 2017.
62. C. Herrojo, J. Mata-Contreras, F. Paredes, A. Núñez, E. Ramon, and F. Martín "Near-field chipless-RFID system with erasable/programmable 40-bit tags inkjet printed on paper substrates", *IEEE Microw. Wireless Compon. Lett.*, vol. 28, pp. 272- 274, Mar. 2018.
63. C. Herrojo, J. Mata-Contreras, F. Paredes, A. Núñez, E. Ramon, and F. Martín, "Very Low-Cost 80-Bit Chipless-RFID Tags Inkjet Printed on Ordinary Paper," *Technologies*, vol. 6, no. 2, p. 52, May 2018.

64. C. S. Hartmann, “A global SAW ID tag with large data capacity,” in Proc. of *IEEE Ultrasonics Symposium*, October 2002, vol. 1, pp. 65–69.
65. N. Saldanha, D.C. Malocha, “Design Parameters for SAW multi-tone frequency coded reflectors” *2007 IEEE Ultrasonics Symp*., pp. 2087-2090, 2007.
66. S. Harma, V.P. Plessky, C.S. Hartmann, W. Steichen, “Z-path SAW RFID tag” *IEEE Trans. Ultrasonics, Ferroelectric Freq. Control*, vol. 55, pp. 208-213, 2008.
67. H. Tao, W. Weibiao, W. Haodong, S. Yongan, “Reflection and scattering characteristics of reflectors in SAW tags”, *IEEE Trans. Ultrasonics, Ferroelectric Freq. Control*, vol. 55, pp. 1387-1390, 2008.
68. S. Harma, V.P. Plessky, L. Xianyi, P. Hartogh, “Feasibility of ultra-wideband SAW RFID tags meeting FCC rules” *IEEE Trans. Ultrasonics, Ferroelectric Freq. Control*, vol. 56, pp. 812-820, 2012.
69. E. Shamonina, V.A. Kalinin, K.H. Ringhofer, and L. Solymar, “Magneto-inductive waveguide”, *Electron. Lett*., vol. 38, pp. 371–373, 2002.
70. J. Naqui, F. Martín, “Application of broadside-coupled split ring resonator (BC-SRR) loaded transmission lines to the design of rotary encoders for space applications“, *IEEE MTT-S Int. Microw. Symp*. (IMS’16), San Francisco, May 2016.
71. J. Mata-Contreras, C. Herrojo, F. Martín, "Application of split ring resonator (SRR) loaded transmission lines to the design of angular displacement and velocity sensors for space applications", *IEEE Trans. Microw. Theory Techn.*, vol. 65, no. 11, pp. 4450-4460, Nov. 2017.
72. M. Polivka, J. Havlicek, M. Svanda and J. Machac, "Improvement in robustness and recognizability of RCS response of U-shaped strip-based chipless RFID tags," *IEEE Ant. Wireless Propag. Lett.*, vol. 15, pp. 2000-2003, 2016.
73. H. Chen, L. Ran, J. Huangfu, X. Zhang, K. Chen, T. M. Grzegorczyk, and J. A. Kong, “Left-handed materials composed of only S-shaped resonators,” *Phys. Rev. E*, vol. 70, no. 5, p. 057605, Nov. 2004.
74. H. Chen, L. Ran, J. Huangfu, X. Zhang, K. Chen, T. M. Grzegorczyk, and J. A. Kong, “Negative refraction of a combined double S-shaped metamaterial,” *Appl. Phys. Lett.*, vol. 86, no. 15, p. 151909, 2005.
75. H. Chen, L.-X. Ran, H.-F. Jiang Tao, X.-M. Zhang, K.-S. Cheng, T. M Grzegorczyk, and J. A. Kong, “Magnetic properties of S-shaped split ring resonators,” *Prog. Electromagn. Res.*, vol. 51, pp. 231–247, 2005.
76. J. Naqui, J. Coromina, A. Karami-Horestani, C. Fumeaux, and F. Martín, “Angular displacement and velocity sensors based on coplanar waveguides (CPWs) loaded with S-shaped split ring resonator (S-SRR)”, *Sensors*, vol. 15, pp. 9628-9650, 2015.
77. M. H. Zarifi, S. Deif, and M. Daneshmand, “Wireless passive RFID sensor for pipeline integrity monitoring,” *Sensors Actuators A Phys.*, vol. 261, pp. 24–29, Jul. 2017.
78. X. Yang et al., "Array waveguide probe loaded with split-ring resonators for sizing the cracks in metal surface," *IEEE Microw. Wireless Compon. Lett*., vol. 28, no. 2, pp. 171-173, Feb. 2018.
79. M. H. Zarifi and M. Daneshmand, "High-resolution RFID liquid sensing using a chipless Tag," *IEEE Microw. Wireless Compon. Lett.*, vol. 27, no. 3, pp. 311-313, Mar. 2017.
80. S. Karuppuswami, L. L. Matta, E. C. Alocilja and P. Chahal, "A wireless RFID compatible sensor tag using gold nanoparticle markers for pathogen detection in the liquid food supply chain," *IEEE Sensors Lett.*, vol. 2, no. 2, pp. 1-4, Jun. 2018.
81. N. M. Cerón Hurtado, M. H. Zarifi, M. Daneshmand and J. Aguiló Llobet, "Flexible microdisplacement sensor for wearable/ implantable biomedical applications," *IEEE Sensors J.*, vol. 17, no. 12, pp. 3873-3883, Jun. 15.
82. P. Vélez, L. Su, K.Grenier, J. Mata-Contreras, D. Dubuc, and F. Martín, "Microwave microfluidic sensor based on a microstrip splitter/combiner configuration and split ring resonators (SRRs) for dielectric characterization of liquids", *IEEE Sensors J.*, vol. 17, no. 20, pp. 6589-6598, Oct. 2017.
83. L. Su, J. Mata-Contreras, P. Vélez, A. Fernández-Prieto, and F. Martín, "Analytical method to estimate the complex permittivity of oil samples", *Sensors*, 18, no. 4, pp. 984, Apr. 2018.
84. F. Costa *et al*., "A depolarizing chipless RF label for dielectric permittivity sensing," *IEEE Microw. Wireless Compon. Lett.*, vol. 28, no. 5, pp. 371-373, May 2018.
85. F. Paredes, C. Herrojo, J. Mata-Contreras, M. Moras, A. Núñez, E. Ramon and F. Martín, “Near-field chipless radio-frequency identification (RFID) sensing and identification system with switching reading”, *Sensors*, vol. 18, pp. 1148, 2018.

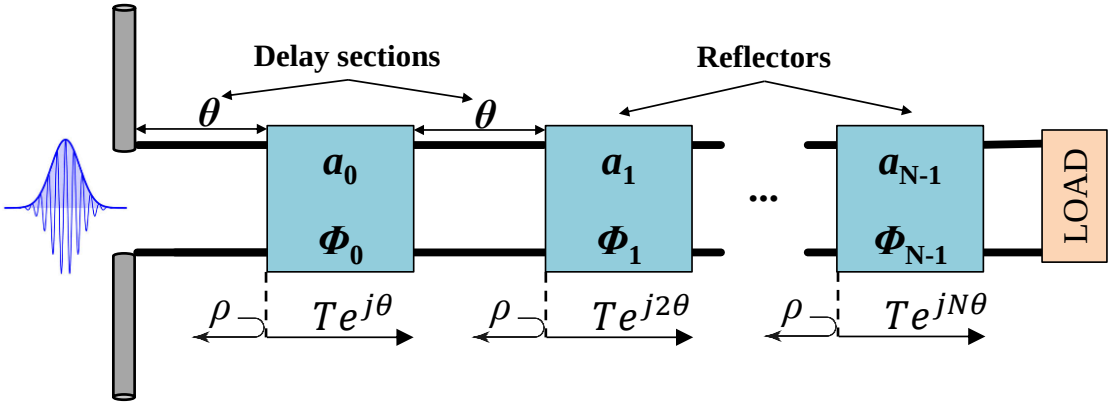

Figure 1. Working principle of chipless-RFID systems based on time-domain reflectometry (TDR).

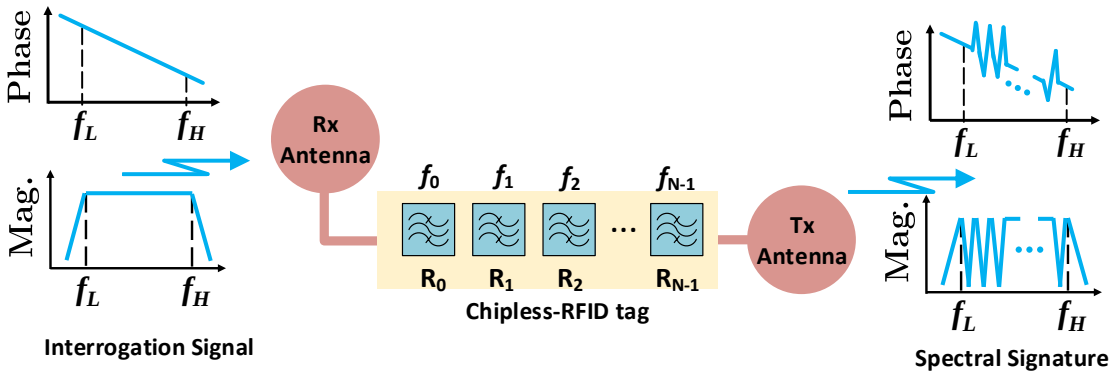

(a)

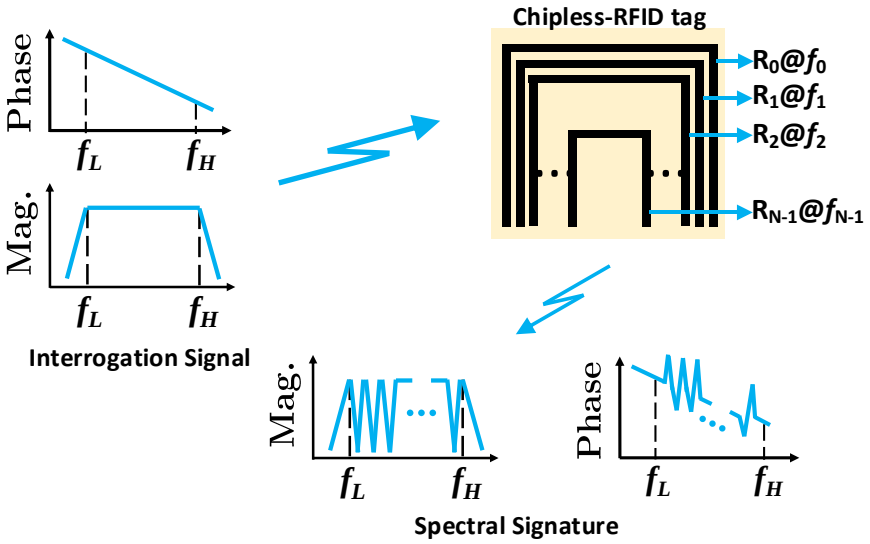

(b)

Figure 2. Working principle of retransmission (a) and backscattered (b) frequency-domain chipless-RFID systems.

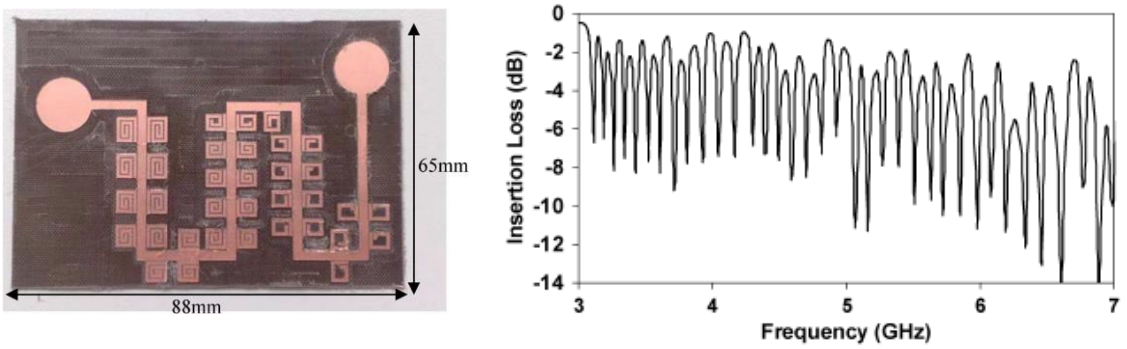

(a) (b)

Figure 3. Photograph (a) and measured response (b) of a 35-bit retransmission based chipless-RFID tag implemented by means of spiral resonators, where all bits are set to '1'. Reprinted with permission from [27]; copyright 2009 IEEE.

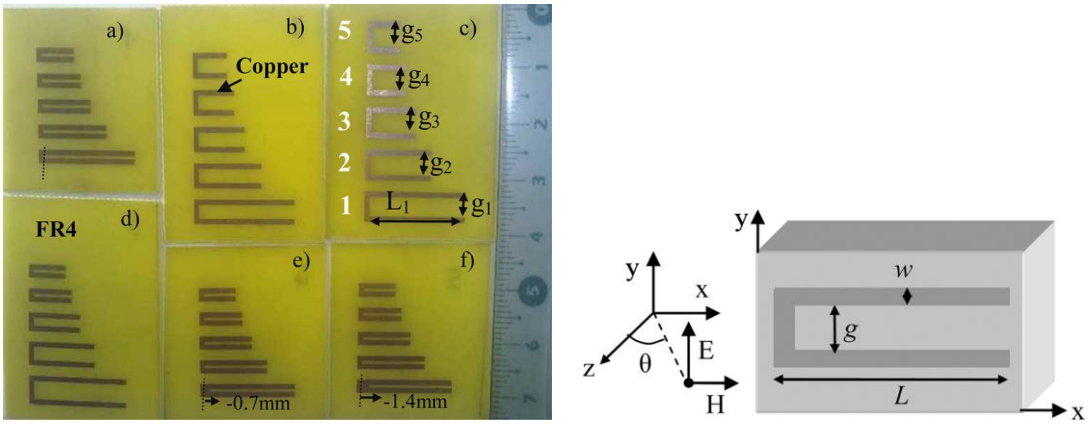

(a) (b)

Figure 4. Photograph of six chipless-RFID tags based on frequency position and phase deviation (a) and topology of the C-shaped resonant element with relevant dimensions and polarization indicated (b). Reprinted with permission from [43]; copyright 2011 IEEE.

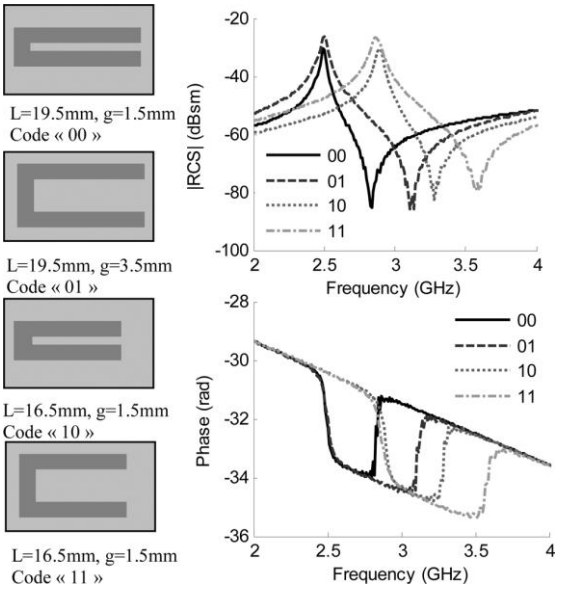

Figure 5. Responses achieved with a single C-shaped resonator (corresponding to two bits), inferred by varying the dimensions, as indicated. Reprinted with permission from [43]; copyright 2011 IEEE.

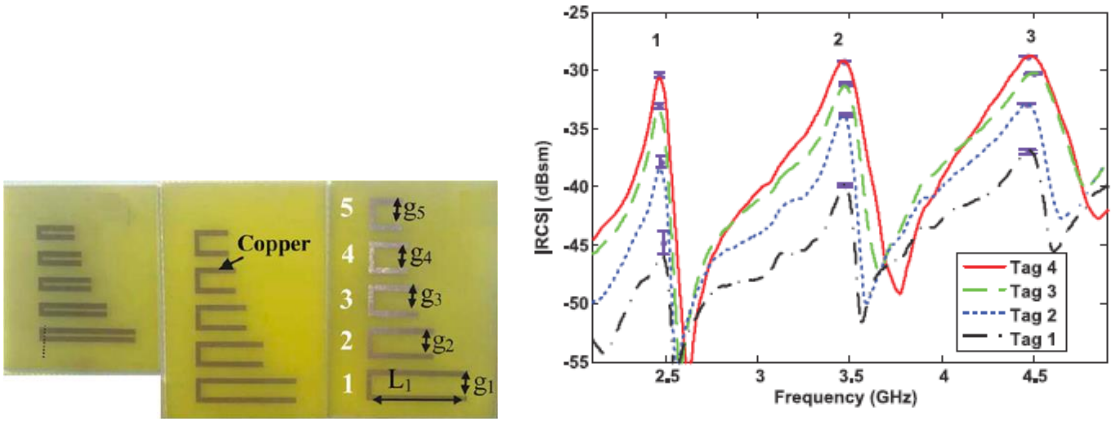

(a) (b)

Figure 6. Photograph of three chipless-RFID tags based on frequency position and RCS peak magnitude (a) and measured response (b). Reprinted with permission from [49]; copyright 2016 IEEE.

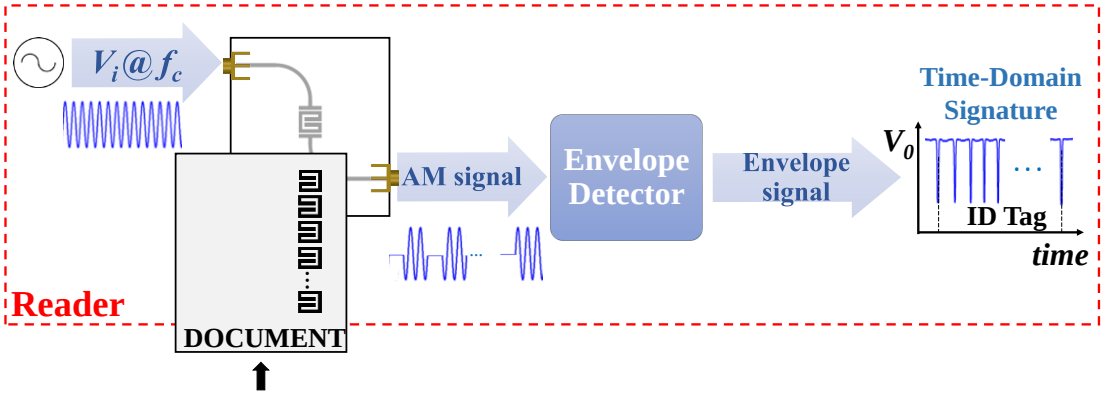

Figure 7. Working principle of time-domain chipless-RFID systems based on near-field coupling and sequential bit reading.

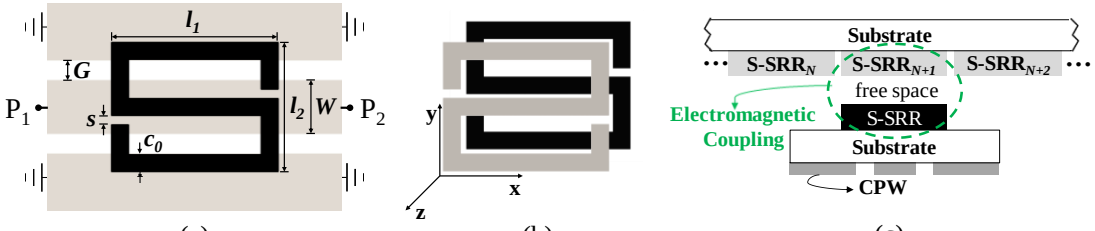

(a) (b) (c)

Figure 8. Layout of the square shaped S-SRR coupled to a CPW transmission line (a), 3D view of the broadside coupled S-SRR (BC-S-SRR) (b), and cross-sectional view of the S-SRR-loaded CPW (reader) with an S-SRR based chipless tag on top of it (c). Dimensions are (in mm) W = 1.2 and G = 0.48, l_1 = 3.8, l_2 = 2.96, c_0 = 0.4, s = 0.2. CPW transmission line and tag are separated by a 0.25 mm air gap. The distance between adjacent S-SRRs (if they are present) in the tag chain is 0.2 mm. For the CPW, the considered substrate is the *Rogers RO3010* with dielectric constant ε_r = 10.2 and thickness h = 0.635 mm. For the tag chain the considered substrate is the *Rogers RO4003C* with dielectric constant ε_r = 3.55 and thickness h = 0.204 mm.

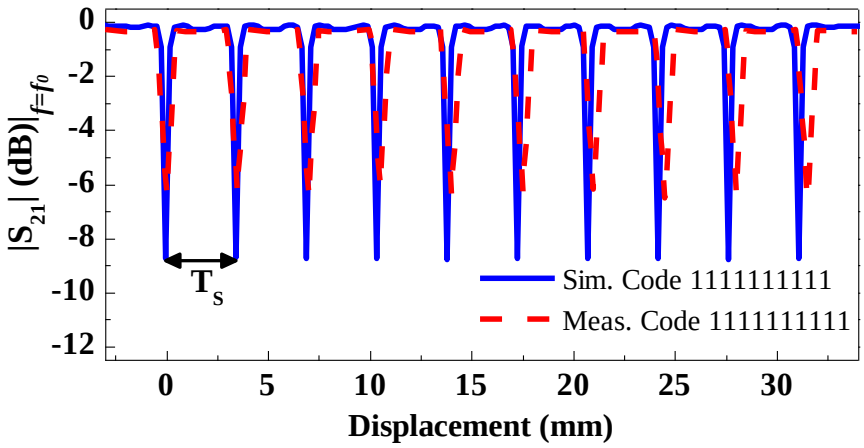

Figure 9. Measured and simulated (inferred from the electromagnetic simulator *Keysight Momentum*) magnitude of the transmission coefficient at f_c, as the linear 10-bit tag is displaced above the S-SRR-loaded CPW transmission line, by considering an air gap of 0.25 mm. Reprinted with permission from [57]; copyright 2017 IEEE.

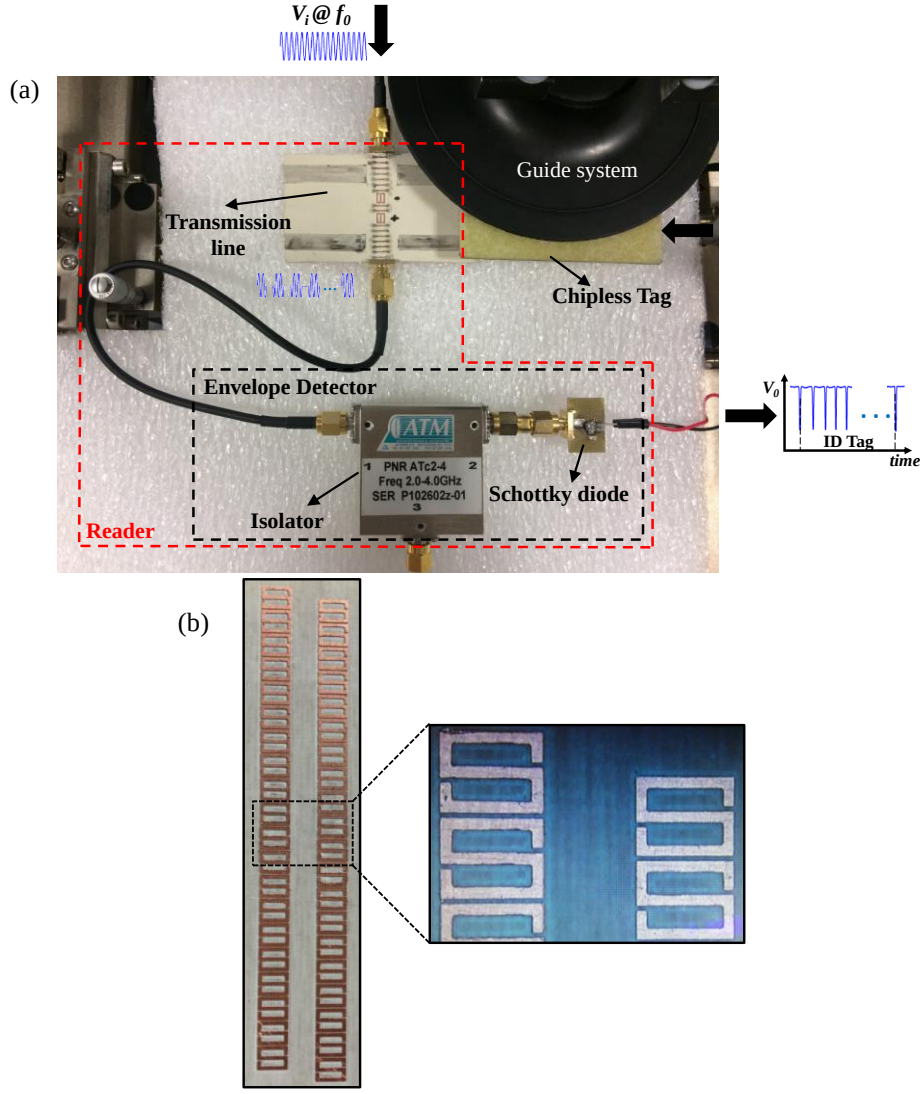

Figure 10. Photograph of the experimental set-up (a) and fabricated double-chain tag with all bits set to the logic state '1' (b). The size of the tag is 11.2 mm × 64.5 mm. Reprinted with permission from [60]; copyright 2017 EDP Sciences.

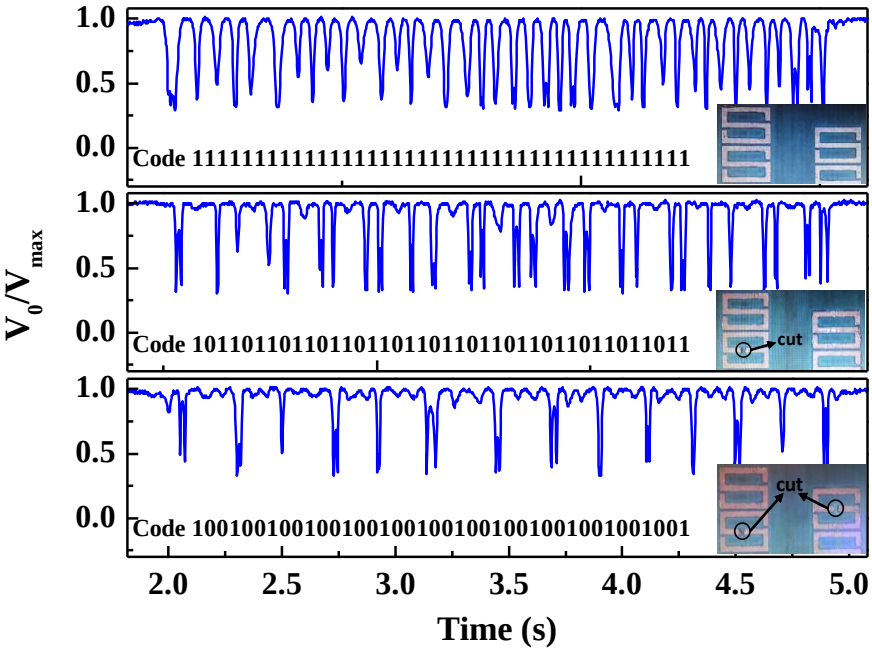

Figure 11. Measured normalized envelope of the 40-bit tags with the indicated codes. Reprinted with permission from [60]; copyright 2017 EDP Sciences.

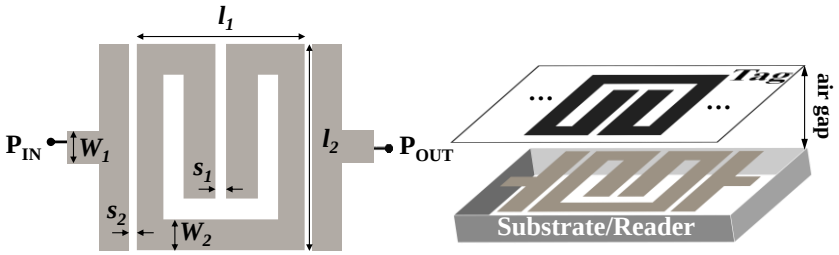

(a) (b)

Figure 12. Layout of the topology of the reader based on a SRR-loaded microstrip line in bandpass configuration (a) and 3D view of the loaded reader with one of the SRRs of the tag perfectly aligned with the SRR of the reader (b). Dimensions are (in mm): l_1 = 3.16, l_2 = 3.35, s_1 = 0.2, s_2 = 0.2, W_1 = 0.56, and W_2 = 0.5. The distance between adjacent SRRs (if they are present) in the tag chain is 0.2 mm. For the reader, the considered substrate is the *Rogers RO3010* with dielectric constant ε_r = 10.2 and thickness h = 0.635 mm. For the tag chain the considered substrate is the *Rogers RO4003C* with dielectric constant ε_r = 3.55 and thickness h = 0.204 mm.

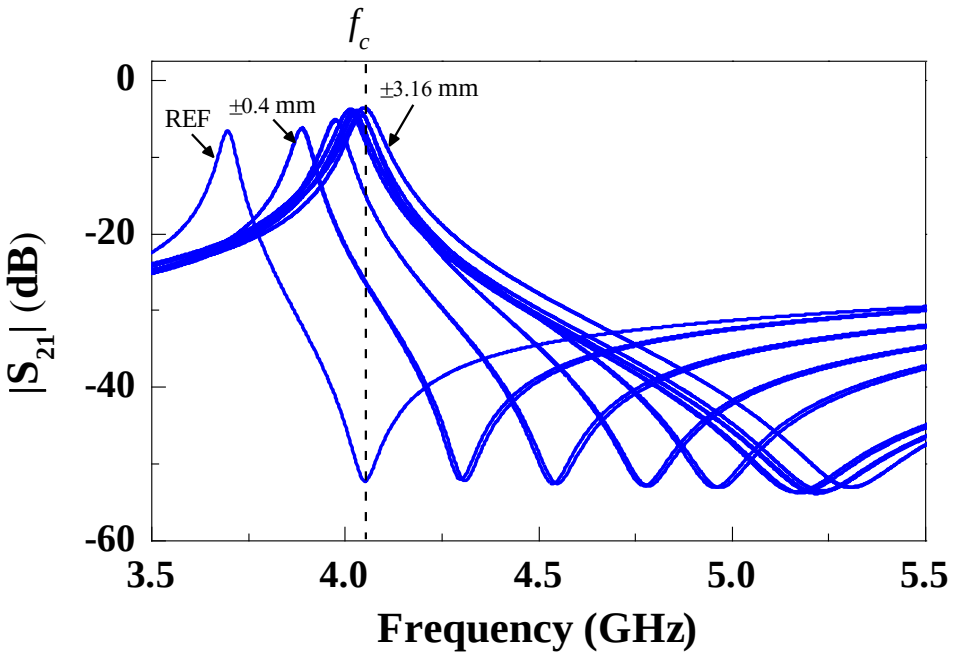

Figure 13. Transmission coefficient (magnitude) of the SRR-loaded line of Fig. 12 with tag cover, for different relative positions between the SRR of the line and the SRR of the tag. These results have been inferred by electromagnetic simulation using *Keysight Momentum*. Reprinted with permission from [61]; copyright 2017 IEEE.

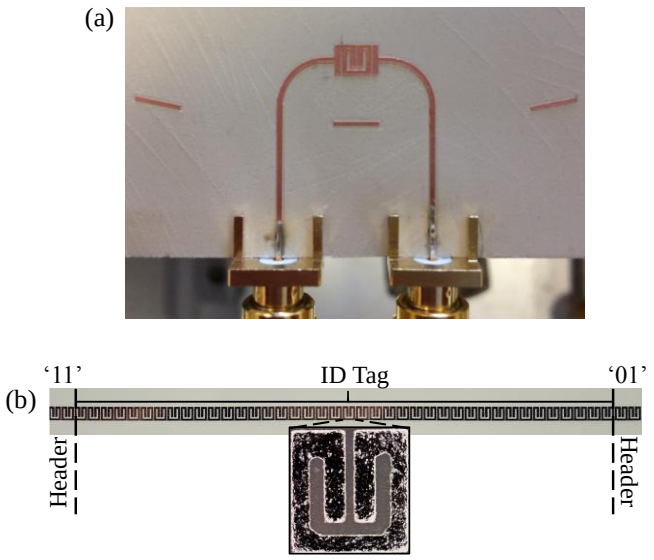

Figure 14. Photograph of the fabricated SRR-loaded microtrip line for tag reading (a) and 40-bit tag with header bits implemented on paper substrate (with all bits set to the logic state '1') (b). The size of the tag is 3.35 mm × 147.6 mm.

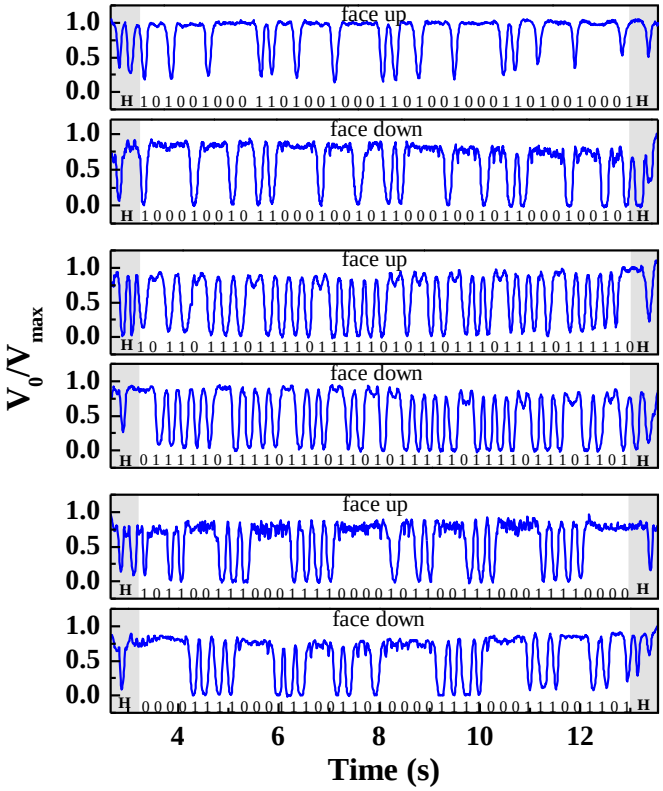

Figure 15. Measured normalized envelope for the 40-bit programmed tags with the indicated codes and with header bits. Reprinted with permission from [62]; copyright 2018 IEEE.

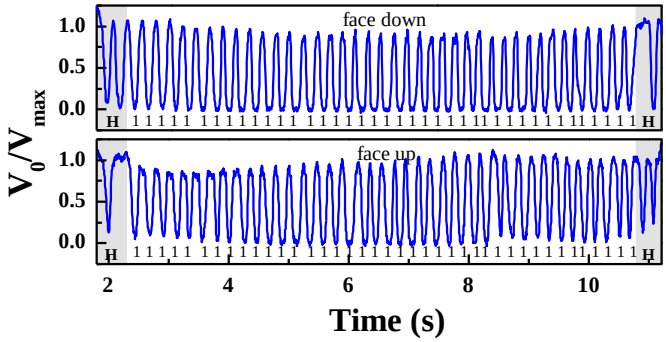

Figure 16. Measured normalized envelope for the 40-bit erased tag with header bits. Reprinted with permission from [62]; copyright 2018 IEEE.

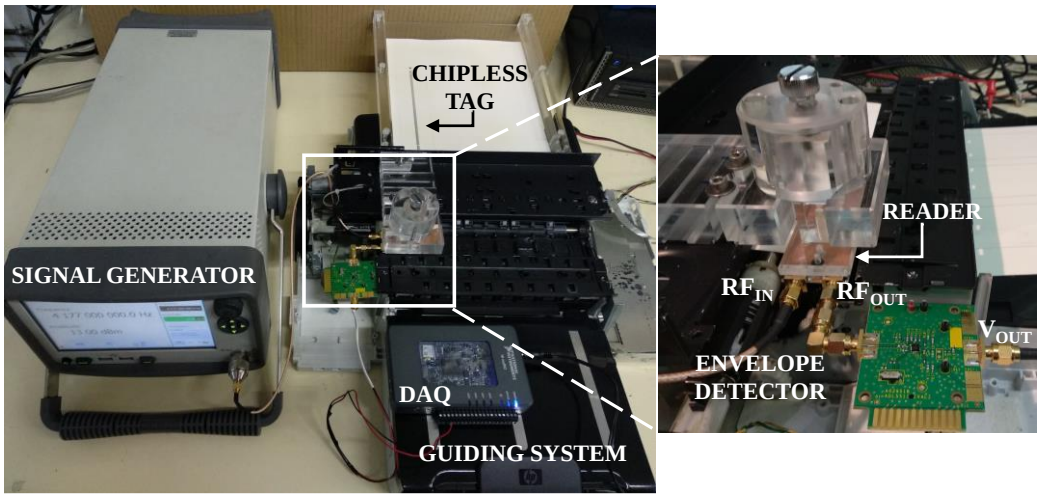

Figure 17. Photograph of the experimental set-up used for obtaining the tag responses (envelope functions) in those tags printed on DIN A4 paper.

Figure 18. Photograph of the 80-bit tag with header bits implemented on ordinary DIN A4 paper (with all bits set to the logic state '1'). The size of the tag is 3.35 mm × 281.9 mm.

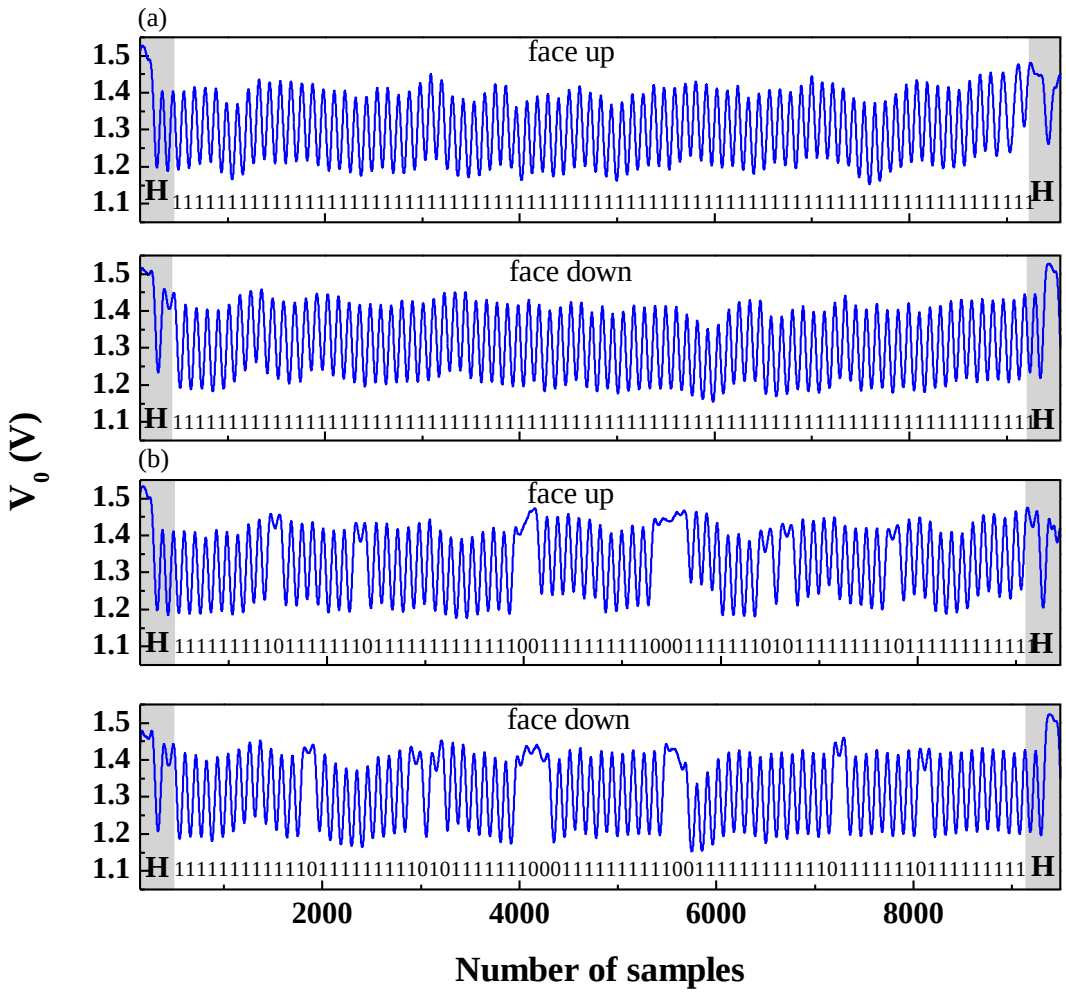

Figure 19. Measured envelope of the inkjet-printed (a) 80-bit tag with all bits set to the logic state '1' and (b) 80-bit programmed tag with the indicated code and with header bits. Since the envelope function has been inferred from a data acquisition system in this second validation experimental set-up, the abscise axis is the number of samples, rather than the time. Reprinted with permission from [63]; copyright 2018 mdpi.